Ruthenium(II) Catalyzed C-H Functionalization Using the Oxazolidinone Heterocycle as a Weakly Coordinating Directing Group: Experimental and Computational Insights.

Jamie A. Leitch,[†] Philippe B. Wilson,[†] Claire L. McMullin,[*,†] Mary F. Mahon,[†] Yunas Bhonoah,[‡] Ian H. Williams[*,†] and Christopher G. Frost.[*,†]

[†]Department of Chemistry, University of Bath, Claverton Down, Bath, Somerset, BA2 7AY, United Kingdom

[‡]Syngenta, Jealott's Hill International Research Centre, Bracknell, Berkshire, RG42 6EY, United Kingdom

KEYWORDS: C-H Activation, Homogeneous Catalysis, Ruthenium, Heterocycles, Kinetic Isotope Effect, DFT

ABSTRACT: Herein reports the ruthenium-catalyzed *ortho*-C-H alkenylation of a wide range of *N*-aryloxazolidinone scaffolds. Alkenylation was achieved with complete mono-selectivity with a scope of 27 examples in 2-MeTHF. Yields ranged from 23-94% creating highly decorated oxazolidinone scaffolds. A kinetically relevant C-H cleavage was also observed with a KIE ~ 2. DFT calculations elucidated information on mechanism, detailing the β-hydride elimination as the most energetically challenging step of +13.5 kcalmol^{-1}. In-depth computational kinetic studies also predicted a KIE of 2.17 for C-H cleavage and an intrinsic KIE for the reaction of 2.22, in line with the experimentally observed value.

INTRODUCTION

The oxazolidinone heterocycle is prevalent in pharmaceutically active compounds with widespread bioactivity for example Linezolid[1], Tedizolid[2] (antibacterial, Figure 1), Rivaroxaban[3] (anti-coagulant) and Toloxatone[4] (antidepressant). For these reasons the synthesis of these heterocycles and their modification has received great attention in recent years.[5] These biologically active structures contain the oxazolidinone heterocycle neighboring an aromatic ring. This makes these structures prime for investigation as directing groups in C-H functionalization catalysis.

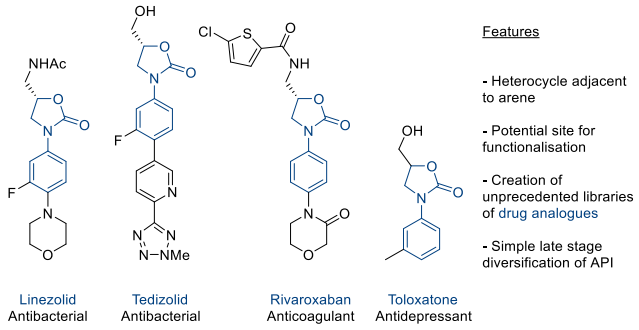

Figure 1: Pharmacologically active compounds containing the oxazolidinone heterocycle.

Transition metal catalyzed C-H functionalization has become a vital synthetic tool to facilitate the formation of useful C-C and C-X bonds.[6] This methodology transforms latent C-H bonds into potentially reactive functional groups. Harnessing this concept to allow derivatization of biologically active compounds such as the oxazolidinones is a very attractive strategy to enable the synthesis of drug analogues through expedient late-stage modification.[7]

Ruthenium catalyzed C-H bond functionalization has seen widespread application into the modern synthetic world due to pioneering developments from Oi and Inoue, Ackermann, and Bruneau and Dixneuf[8]. Methodology has evolved rapidly to utilize weakly coordinating carbonyl directing groups to install diverse functionality.[9] This functionality is often ubiquitous in chemical structures; however, if necessary, an auxiliary approach can be used which involves separate installation and removal steps.[9k] The presented study is focused on the utility of directing groups with intrinsic biological activity and how they facilitate C-H insertion via chelation assistance (Scheme 1). Despite early work reporting palladium catalyzed *ortho*-arylation of the 3-aryl-2-oxazolidinone structure, the motif has not been widely used as a directing group and there have been no such examples employing ruthenium catalysis.[10]

Scheme 1: Ruthenium Catalyzed Alkenylation of Arenes

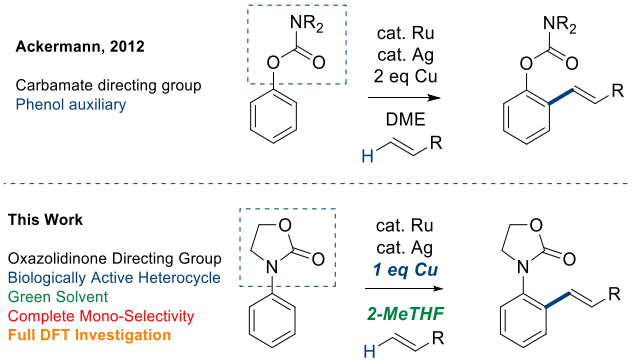

RESULTS & DISCUSSION

Optimization

The envisioned reaction methodology was probed using 3-phenyl-2-oxazolidinone (**1a**) and ethyl acrylate (**2a**). The electron deficient nature of acrylates has shown them to be excellent coupling partners in ruthenium, palladium and rhodium catalyzed C-H functionalization reactions.[9a,11] A summary of the optimization is displayed in Table 1.

Table 1: Optimization of Oxazolidinone Directed C-H Alkenylation[a]

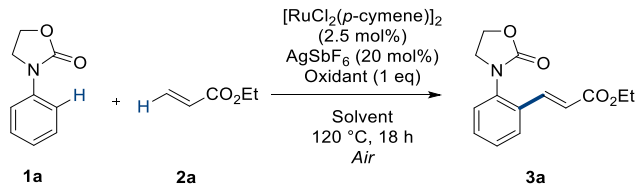

1a **2a** **3a**

Entry	Solvent	Oxidant	**3a**[b]
1	DCE	$Cu(OAc)_2$	15
2	1,4-dioxane	$Cu(OAc)_2$	56
3	DME	$Cu(OAc)_2$	72 (68)[c]
4	2-MeTHF	$Cu(OAc)_2$	70 (67)[c]
5	2-MeTHF/AcOH 3:1	$Cu(OAc)_2$	-
6	2-MeTHF	Ag_2CO_3	13
7	2-MeTHF	AgOAc	48
8	2-MeTHF	AgOAc[d]	64
9	2-MeTHF	AgO_2CCF_3	Trace
10	2-MeTHF	$Cu(OAc)_2{\cdot}H_2O$	77
11[e]	2-MeTHF	$Cu(OAc)_2{\cdot}H_2O$	-
12[f]	2-MeTHF	$Cu(OAc)_2{\cdot}H_2O$	-
13[g]	2-MeTHF	$Cu(OAc)_2{\cdot}H_2O$	68
14[h]	2-MeTHF	$Cu(OAc)_2{\cdot}H_2O$	78
15[h,i]	**2-MeTHF**	**$Cu(OAc)_2{\cdot}H_2O$**	**80 (76)**[c]

[a]General Reaction Conditions: **1a** – 1 mmol, **2a** – 3 mmol, $[RuCl_2(p\text{-cymene})]$ (2.5 mol%), $AgSbF_6$ (20 mol%), Solvent (4 mL). [b] ^1H NMR conversion. [c]Isolated Yields after purification. [d]AgOAc (2 eq). [e]Without $[RuCl_2(p\text{-cymene})]_2$. [f]Without $AgSbF_6$. [g]Reaction performed at 100 °C [h]$AgSbF_6$ (10 mol%). [i]Solvent (1 mL)

Starting conditions were obtained from literature precedent for the use of ruthenium, silver and copper in cooperative catalysis for similar transformations (full optimization information is available in the supporting information).[9f,h,i,k] Alkenylation was observed DCE in low conversions (entry1). Much more substantial formation of product was observed with higher boiling polar aprotic etheric solvents (1,4-dioxane, DME and 2-MeTHF, entries 2-4). A 2-MeTHF/AcOH mixture was interestingly shown to completely nullify reactivity (entry 5) as AcOH is a proposed by-product in the reaction. 2-MeTHF was carried forward as solvent as choice as is a more sustainably sourced alternative to DME.[12]

Multiple silver(I) oxidants were investigated with none showing superior activity to $Cu(OAc)_2$ (entries 6-9). However, the mono-hydrate complex was not only tolerated but shown to accelerate catalysis (entry 10). Only oxidants containing carboxylate counter ions promoted the reaction. This is in line with literature precedent for a concerted metalation-deprotonation (CMD) or ambiphilic metal-ligand activation (AMLA) mechanism of C-H metalation.[6a,b]

It must be noted that reaction efficacy was not maintained in the absence of either ruthenium catalyst or silver co-catalyst (entries 11-12), however it was possible to decrease silver co-catalyst loading without detriment to the reaction (entry 14). Finally, the reaction was shown to proceed with equal if not superior reactivity at higher concentration and proceeding with excellent catalytic efficiency under air (entry 15). Here oxygen in the atmosphere aids oxidant recycling.[8a] Also noteworthy was that throughout this optimization there was no observation of *o*-,*o*-di-alkenylated product either by NMR or TLC. This high level of selectivity is an attractive feature.[6b, 8a]

Reaction Scope

With optimized conditions in hand, 3-phenyl-2-oxazolidinone (**1a**) was reacted with a variety of electron deficient and electron rich alkenes to explore the scope of this catalytic transformation (Scheme 2).

Scheme 2: Acrylate Scope of Oxazolidinone Directed C-H Alkenylation

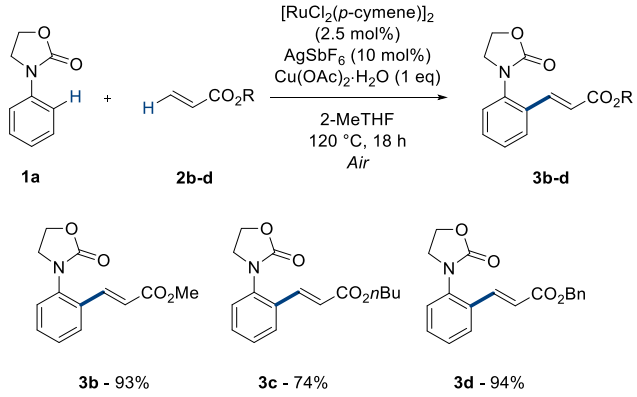

1a **2b-d** **3b-d**

3b - 93% **3c** - 74% **3d** - 94%

Excellent catalytic activity was maintained using methyl, *n*-butyl and benzyl acrylates showing yields up to 94%. Unfortunately the reaction did not proceed with other electron deficient alkenes and electron rich alkenes due to lack of reactivity or high volatility of substrates in open atmosphere (see supporting information). Despite this, similar structures can be accessed from **3a-d** through functional group interconversions. The use of methyl acrylate enabled more facile purification *via* standard chromatographic methods (cf. benzyl) as well as superior isolated yields (cf. ethyl). Due to this, methyl acrylate was carried forward as the acrylate of choice for expansion of the scope with aryl oxazolidinones (Scheme 3).

The reaction was shown to tolerate a wide variety of functionality on the aryl ring including fluoro-, chloro-, bromo-, alkoxy-, aryl, and alkyl. Highest yields were achieved using electron rich substituents (**3ab**, **3ac**, **3ai**, **3aj**). Yields were reduced when using highly electron deficient arenes with substituents such as CF_3 or *m*-*p*-Cl (**3ag** & **3an**). These patterns in reaction efficiency are consistent with similar reported methodology.[8k] Unsymmetrical examples such as 3-methyl and 3-chloro (**3ai**-**3an**) gave major isomers based on the least sterically hindered site with excellent selectivity. An *ortho*-substituted example (**3ao**) was also tolerated however in reduced yield. Heteroaromatics could also be functionalized with excellent efficiency demonstrated with thiophene derivative (**3ap**).

Scheme 3: Arene Scope of Oxazolidinone Directed C-H Alkenylation

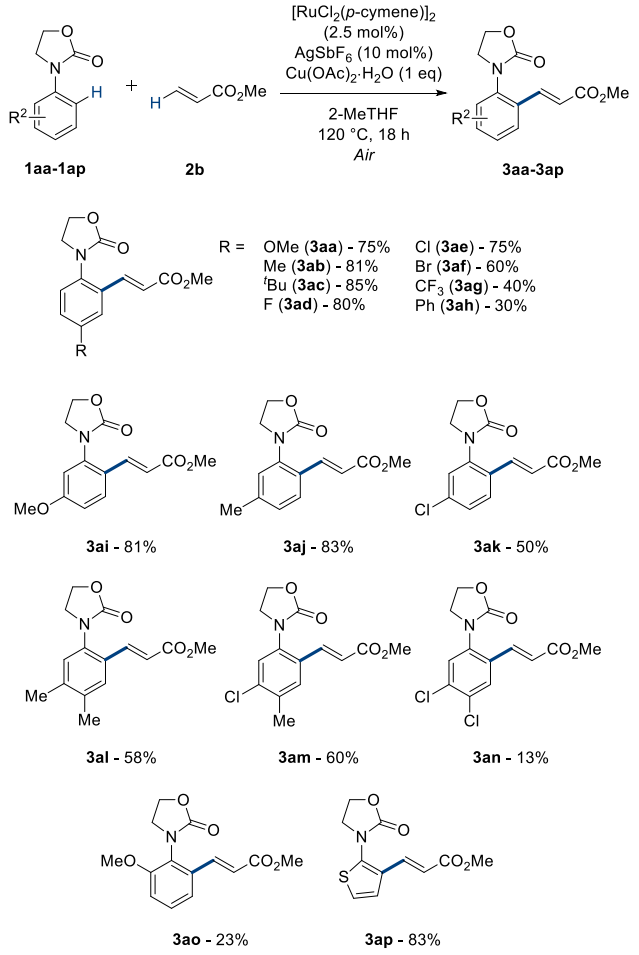

Structures bearing a fluoro substituent *meta*- to the oxazolidinone directing group (**3aq** & **3ar**) gave a mixture of regioisomers (Scheme 4), separable *via* column chromatography.

Scheme 4: Oxazolidinone Directed C-H Alkenylation of Structures Bearing *meta*-Fluoro Substituent

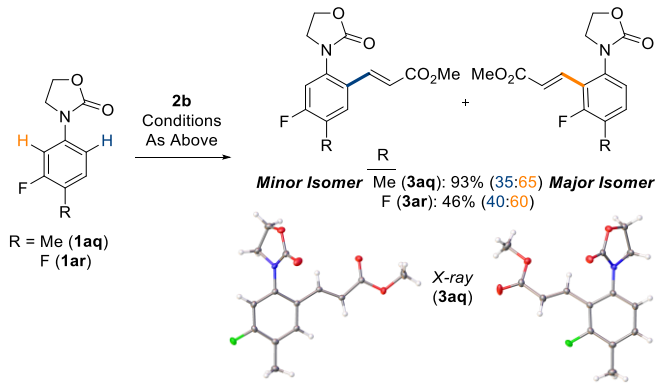

Regioisomers of structure **3aq** gave an impressive combined yield of 91% and were further characterized by single crystal X-ray crystallography to confirm regiochemistry.[13] These validated that the electronics of the system dictate the selectivity in these structures. This insight in selectivity is mirrored in a previous report in a benzamide assisted C-H cyanation reaction.[14]

3ar gave a similar distribution of C-H alkenylated products with comparable isomer ratios albeit in lower yield.

Functionalization of the heterocycle itself was then varied using structures synthesized from natural amino acids valine and leucine (Scheme 5a). These substrates performed with good efficiency for such highly functionalized motifs. Yields were reduced with larger alkyl derivatives due to potential disruption of directing group C-H alignment, highlighted with **3bd**.

Methanol derivative (**1ca**) bearing functionality in the 5-position was reacted under the catalytic conditions (Scheme 5b). The reaction conditions led to some undesired removal of the silyl protecting group. Due to this, the crude mixture was submitted to an *in situ* deprotection to afford the primary alcohol structure. One pot methodology was pleasingly shown to manifest comparable efficiency to sequential isolation and separate deprotection. This allows for more expedient synthesis and reduced waste from work-up and purification. This methodology now allowed the synthesis of highly decorated oxazolidinone structures.

Scheme 5: Heterocycle Scope of Oxazolidinone Directed C-H Alkenylation

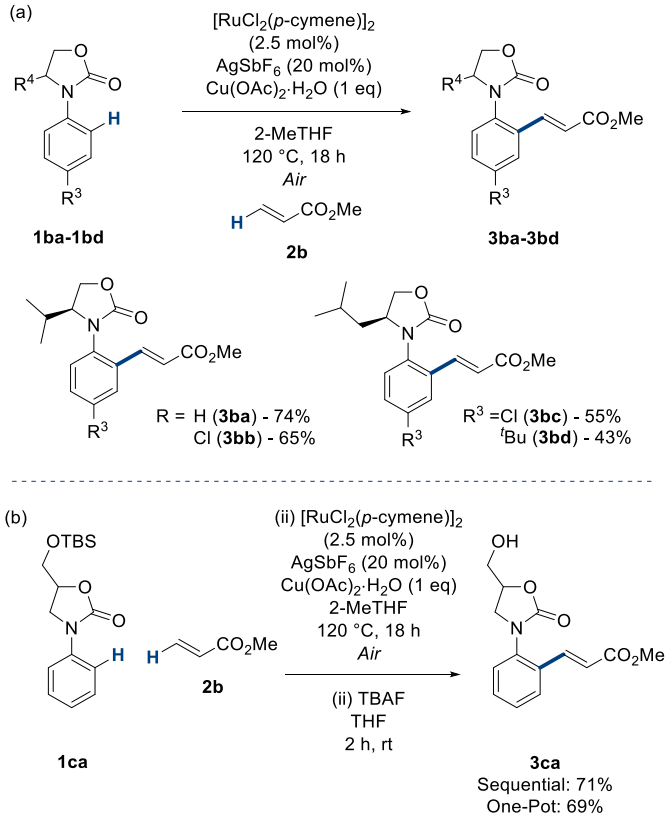

This methodology was shown to be scalable affording over 2 grams' worth of alkenylated product (Scheme 6). On a gram scale the lowering of ruthenium and silver loadings afforded a 77% yield along with a 22% yield of recovered starting material.

Interestingly there was still no observed presence of a di-alkenylated structure, which was also not observed throughout the scope of the reaction. Complete mono-substitution selectivity in C-H functionalization methodology is highly sought after. To investigate this further, mono-alkenylated product **3b** was re-exposed to the optimized reaction conditions in an attempt to

force formation of the di-alkenylated product **3b$_{di}$** (Scheme 7). Despite this, no sign of this product was observed via TLC or crude NMR where only starting material was present. This highlighted the absolute selectivity of the oxazolidinone directing group towards mono-functionalization.

Scheme 6: Gram Scale Ruthenium Catalyzed C-H Alkenylation

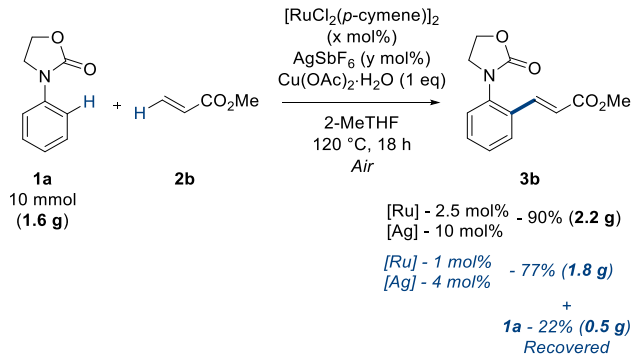

Scheme 7: Attempted Di-Alkenylation of Mono-Substituted Structure 3b

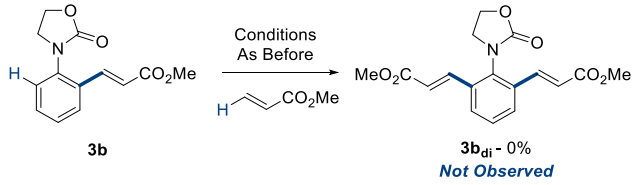

The introduction of ester and alkene functionality to the compound allows further derivation to form more complex and decorated structures. Heterogeneous hydrogenation allowed access to the *ortho*-alkylated motif in quantitative yield (**4a**, Scheme 8). Selective mild saponification allowed hydrolysis of the ester (**4b**) without interaction with the oxazolidinone heterocycle. Amidation conditions also afforded the amide in good yields (**4c**). These functional group interconversions allowed access to cinnamic acids and cinnanamide structures which are known to possess antimicrobial activity.[15]

The reaction conditions were now employed with analogous derivatives of the oxazolidinone heterocycle core to explore electronic effects on efficiency of catalysis (Scheme 9). The pyrrolidinone (**6a**), 2-thiazolidinone (**6b**) and 4-thiazolidinone (**6c**) structures gave modest-good yields in the C-H alkenylation reaction. These results manifest how subtle changes in heterocycle electronics can affect C-H functionalisation efficiency under the same reaction conditions.[10a,16]

Mechanistic Studies

There have been multiple other examples of weak directing groups directing C-H alkenylation reactions such as carboxylic acids[8c] ketones[8i], aldehydes[8f] and esters[8h]. As reported reaction conditions for these protocols are similar, it was of mechanistic interest to perform intermolecular competition experiments to create a reactivity order of directing groups. One equivalent of further weakly coordinating directing groups: ketone, acid, ester and aldehyde (**7a-d**) were reacted under the optimized conditions from this report with one equivalent of 3-phenyl-2-oxazolidinone (**1a**) to compete with one equivalent of methyl acrylate (**2b**) (Scheme 10).

Scheme 8: Further Derivation of Alkenylated 3-Phenyloxazolidinone 3b

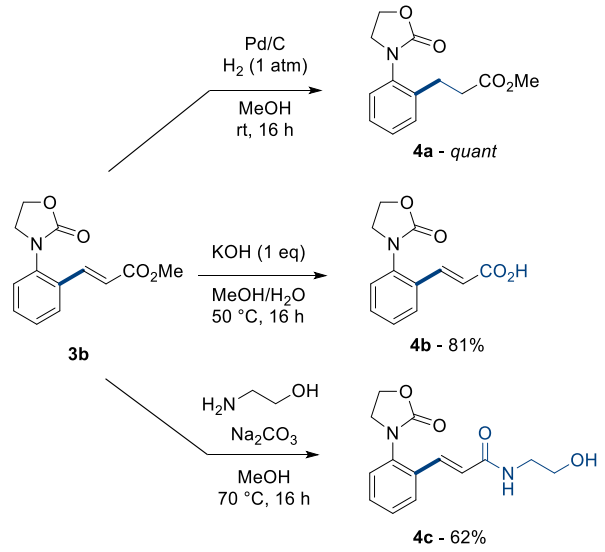

Scheme 9: Ruthenium Catalyzed Alkenylation of 5-Membered Heterocycles

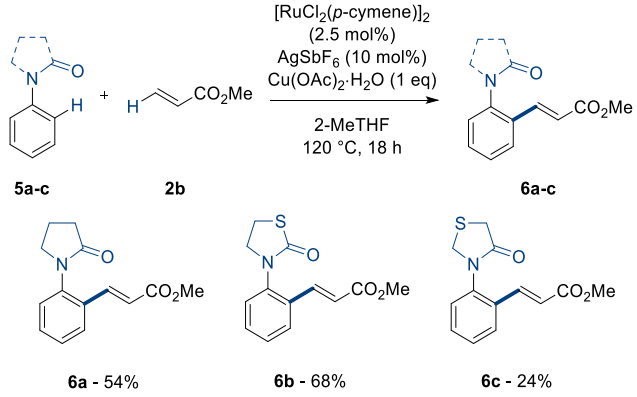

These experimental insights show that the ketone directing group (**7a**) competes preferentially over the oxazolidinone whereas acids, aldehydes and esters give rise to a larger majority of alkenylated aryloxazolidinone. This also allows understanding into potential functional group tolerance of this methodology, where aromatic acyl derivatives of the aryloxazolidinone would give rise to a large mixture of products which was observed experimentally when *para*-acetyl-*N*-aryloxazolidinone was submitted to the reaction conditions.

Silver hexafluoroantimonate ($AgSbF_6$) is a ubiquitous catalytic partner to ruthenium *para*-cymene dimer.[8c,8f] It was of interest to investigate whether it only acts as a catalyst activator or plays a further part in the reaction. Due to this, a proposed catalytically active monomeric species [Ru(*p*-cymene)$(OAc)_2$] was subjected to the reaction conditions with and without the co-catalyst (Scheme 11). Interestingly no conversion to product was observed without the additive, highlighting its further importance as a source of SbF_6^- anion in the reaction.

Scheme 10: Intermolecular Competition Experiments with Weakly Coordinating Directing Groups 7a-d

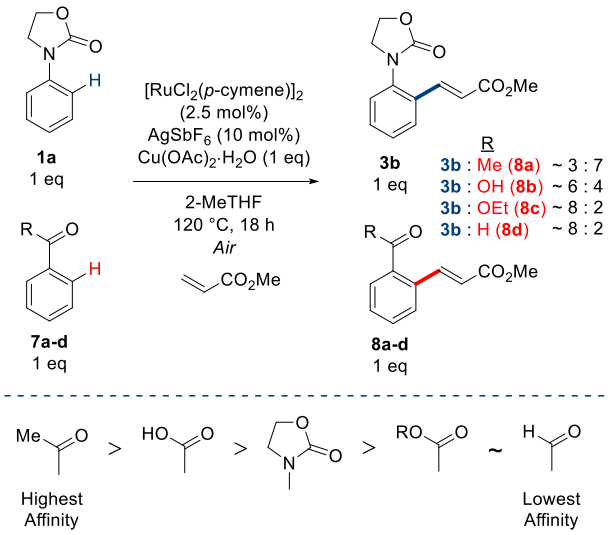

Scheme 11: Ru(II) Catalyzed C-H Alkenylation using a Defined Ruthenium Catalyst Monomer

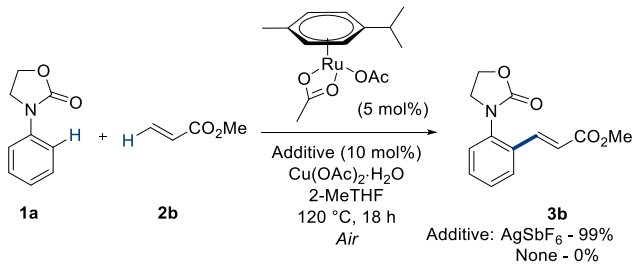

Replacement of the aromatic C-H bonds with deuterium atoms gave the isotopically labelled structure **[D]$_5$-1a**. This was submitted to the reaction conditions in order to investigate the potential hydrogen incorporation into the final product. This would be indicative of a reversible cyclometalation. The resulting reaction gave rise to an 8% hydrogen incorporation into the *ortho*-C-D bond (Scheme 12), also affording the isotopically labelled product in a reduced but still good yield of 69%.

Scheme 12: Ru(II)-Catalyzed Alkenylation of Isotopically Labelled Substrate

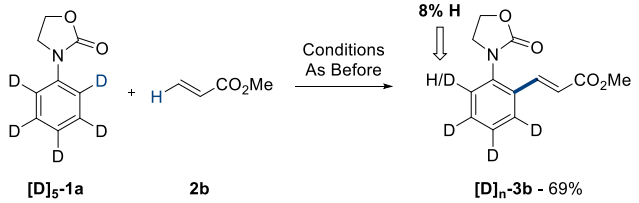

The kinetic isotope effect (KIE) of a substrate can give great insight into mechanism and give information about the rate limiting sections of the catalytic cycle. This allows greater in-depth understanding of reaction tuning and optimization.[17] Kinetic isotope analysis was carried out experimentally using two methods: initial rates by parallel reactions (Scheme 13a) and through intermolecular competition between **1a** and **[D]$_5$-1a** (Scheme 13b). Both methods showed that the reaction had a kinetically relevant isotope effect, signifying that C-H cleavage is in or near the rate limiting step.

Scheme 13: Experimental Investigation of Kinetic Isotope Effect

(a) KIE by Initial Rates using Parallel Reactions

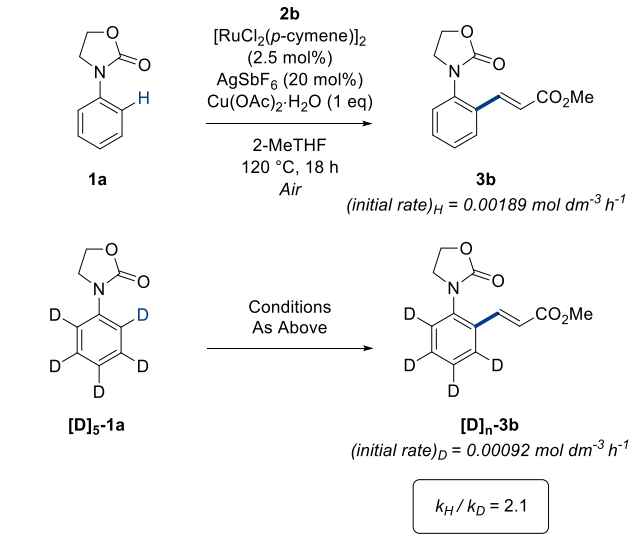

(b) KIE by Intermolecular Competition

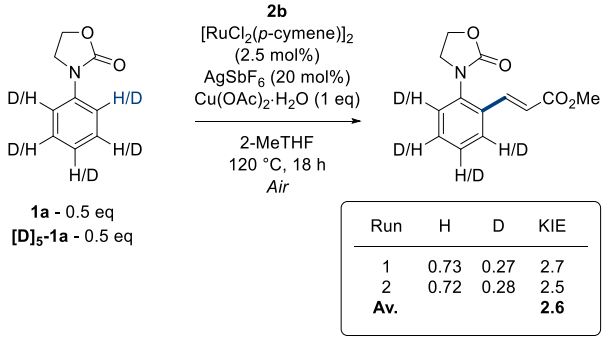

Run	H	D	KIE
1	0.73	0.27	2.7
2	0.72	0.28	2.5
Av.			**2.6**

Computational Mechanistic Studies

Density functional theory (DFT) calculations were undertaken to establish the mechanism and energetics of the reaction for 3-phenyl-2-oxazolidinone **1a** and methyl acrylate **2b**.[18] Previous studies have shown the importance of using corrections for dispersion, solvation and extended basis sets when treating large organometallic reaction systems that involve charged species. A similar approach was adopted in this work, with geometries initially optimized in the gas phase with the BP86 functional and a medium sized basis set (SDD for Ru and 6-31G** on all other atoms). The resultant free energies were then corrected for solvation (2-Me-THF), dispersion (Grimme's D3-BJ parameter set) and an extended basis-set (cc-pVTZ for Ru and 6-311++G** for all other atoms) giving rise to composite free energy differences ΔG_{MeTHF} (1 atm, 25 °C) relative to complex **A** and separate species **1a** and **2b**.

Under the catalytic conditions, acetate from the copper complex ($Cu(OAc)_2{\cdot}H_2O$) breaks up the dimer $[RuCl_2(p\text{-cymene})]_2$ to form the *in situ* catalytically active intermediate **A**, $[Ru(p\text{-cymene})(OAc)(\mathbf{1a})]^+$, with the silver compound ($AgSbF_6$) removing chloride anions from the solution. The cationic complex **A** has the oxazolidinone coordinated through the carbonyl oxygen, one κ^2-acetate and an η^6 *para*-cymene ligand around the ruthenium center. Concerted metalation-deprotonation (CMD), also known as ambiphilic metal-ligand activation

(AMLA), occurs as a two-step reversible process (see Figure 2). The first step, via **TS(A-B)1**, involves κ^2- κ^1 displacement of acetate, by the approaching *ortho* C-H bond of **1a**, to form an agostic intermediate **INT(A-B)**, where the pendant oxygen of the acetate is directed towards the *ortho* H (O···H = 1.686 Å), thereby elongating the C-H bond from 1.091 Å to 1.148 Å. The second step, via **TS(A-B)2**, involves endergonic C-H bond cleavage to form a six-membered cyclometalate **B** (+4.0 kcal mol^{-1}). Formation of the agostic intermediate, which involves breaking a strong Ru-O bond, determines the overall C-H activation barrier of 12.4 kcal mol^{-1}.

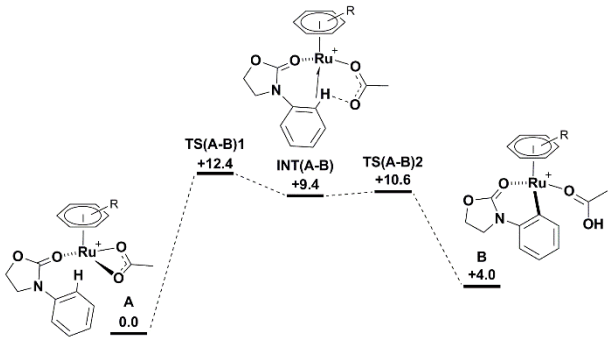

Figure 2: DFT calculated free energies (kcal mol^{-1}) relative to **A** for the C-H activation of *N*-aryloxazolidinone **1a** at [Ru(OAc)(*p*-cymene)]$^+$ in Me-THF.

Ligand substitution of acetic acid in **B** for methyl acrylate **2b** forms four isomers of **C**, which differ with respect to the orientation of the alkene at the ruthenium center. Despite the pre-1,2-insertion intermediates **C1**$_{1,2}$ and **C2**$_{1,2}$ being more stable than the equivalent pre-2,1-insertion intermediates, the free energy barriers for 1,2-insertion (**TS(C1-D1)**$_{1,2}$ and **TS(C2-D2)**$_{1,2}$) are respectively 20.0 and 19.9 kcal mol^{-1}, approximately 5 kcal mol^{-1} higher than 2,1-insertion (see Figure 3 and Figure S1 in the supporting information). Therefore, 2,1-insertion of **2b** into the Ru-C bond is regiosterically favored via **TS(C1-D1)**$_{2,1}$ (13.8 kcal mol^{-1}) and **TS(C2-D2)**$_{2,1}$ (14.9 kcal mol^{-1}), placing the methyl ester substituent next to the ruthenium in the exergonic eight-membered metallacycles either below (**D1**$_{2,1}$; -1.7 kcal mol^{-1}) or above (**D2**$_{2,1}$; -1.3 kcal mol^{-1}) the plane of the ruthenacycle (when looking at the complex from the position of the *para*-cymene ligand).

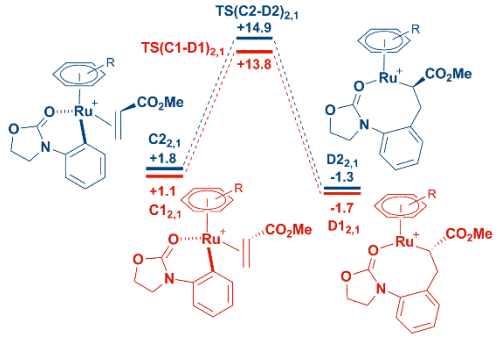

Figure 3: DFT calculated free energies (kcal mol^{-1}) relative to **A** and the free substrates, for the 2,1-insertion of methyl acrylate **2b** into adduct **C**.

Unlike in previous functionalization studies with methyl acrylate (by Davies and Macgregor[19], who used 3-phenyl-pyrazole to form a seven-membered rhodacycle) for this 2,1-insertion no interaction is observed between Ru and the ester substituent in the eight-membered ruthenacycle. In fact, the increased size of the metallacycle restricts its ability to interconvert between conformers **D1**$_{2,1}$ and **D2**$_{2,1}$, as the preference for the boat-chair conformation reduces the flexibility of the metallacycle ring; this contrasts with the behavior that has been reported for similar, yet smaller, equivalent seven-membered intermediates.[19] The stereochemistry of the 1,2-disubstituted alkene product **3b** is determined exclusively by which β-hydrogen is transferred to the ruthenium center; from either above (H_a, Figure 4) or below (H_b) the plane of the ruthenacycle.

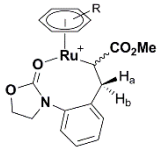

Figure 4: Ruthenacycle **D**$_{2,1}$ showing the position of H_a (above) and H_b (below) the plane of the metallacycle. **D1**$_{2,1}$ has the CO_2Me substituent *cis* to H_b whilst **D2**$_{2,1}$ has the ester group *cis* to H_a

The β-hydrogen transfer process involves two steps: formation of an agostic intermediate followed by C-H cleavage, as the β-H moves to the Ru center. Figure 5 shows the transfer of H_a, which lies above the plane of the ruthenacycle, for both **D**$_{2,1}$ isomers. In the case of **D1**$_{2,1}$, where the transferring hydrogen is *trans* to the ester group, formation of the agostic interaction between H_a and Ru proceeds via **TS(D1-E1)1$_a$** (19.1 kcal mol^{-1}) to give intermediate **INT(D1-E1)$_a$** (+13.1 kcal mol^{-1}), and C-H cleavage occurs via **TS(D1-E1)2$_a$** (13.9 kcal mol^{-1}) to form the *cis* product **E1**$_{cis}$ (+10.4 kcal mol^{-1}). For **D2**$_{2,1}$, with H_a *cis* to the ester group, formation of the agostic interaction proceeds via **TS(D2-E2)1$_a$** (13.5 kcal mol^{-1}), decreasing the Ru···H_a distance from 3.701 to 2.716 Å in **INT(D2-E2)$_a$** (+5.8 kcal mol^{-1}) before C-H cleavage via **TS(D2-E2)2$_a$** (7.8 kcal mol^{-1}) and formation of the experimentally observed *trans* **3b** product [Ru(p-cymene)(**3b**)(H)]$^+$ (**E2**$_{trans}$; +4.9 kcalmol^{-1}).

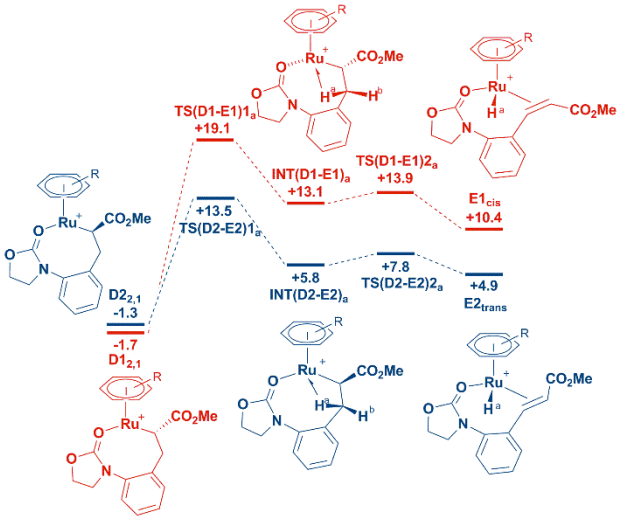

Figure 5: DFT calculated free energies (kcal mol^{-1}) relative to **A** and the free substrates, for the β-H_a transfer from 2,1-insertion ruthenacycles (**D**$_{2,1}$) in Me-THF.

The process of β-H transfer is more complicated for the "bottom" hydrogen, H_b shown in Figure 6, as the formation of the agostic interaction between H_b and Ru (Ru···H_b decreasing to

2.4 Å) forces dissociation of the oxazolidinone group at the ruthenium center (Ru···O increasing to 3.4 Å). This raises the barriers for the first step from **D1$_{2,1}$** via **TS(D1-E1)1$_b$** (17.5 kcal mol^{-1}) and from **D2$_{2,1}$** via **TS(D2-E2)1$_b$** (31.9 kcal mol^{-1})**.** The C-H$_b$ bond is elongating by ~ 0.03 Å as the Ru-H$_b$ distance decreases; this is a greater distortion than C-H$_a$ (~ 0.01 Å) when the agostic intermediate is formed for the top β-H transfer. C-H$_b$ cleavage occurs via **TS(D1-E1)2$_b$** (13.6 kcal mol^{-1}) and **TS(D2-E2)2$_b$** (20.4 kcal mol^{-1}) for **D1** and **D2** respectively to give intermediates **E1′$_{trans}$** (+9.7 kcal mol^{-1}) and **E2′$_{cis}$** (+14.1 kcal mol^{-1}). Reassociation of the oxazolidinone oxygen occurs via **TS(E1′-E1)$_{trans}$** (12.8 kcal mol^{-1}) and **TS(E2′-E2)$_{cis}$** (16.8 kcal mol^{-1}) to form the equivalent **E1$_{trans}$** (+11.3 kcal mol^{-1}) and **E2$_{cis}$** (+14.3 kcal mol^{-1}) complexes, which are less stable than the preceding **E′** complexes.

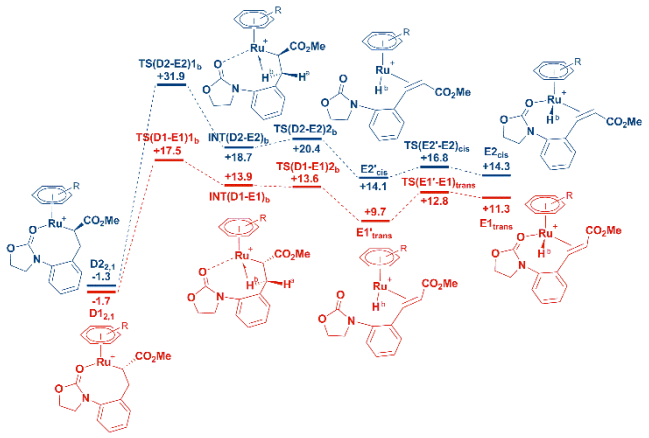

Figure 6: DFT calculated free energies (kcal mol^{-1}) relative to **A** and the free substrates, for the β-H$_b$ transfer from 2,1-insertion ruthenacycles (**D$_{2,1}$**) in Me-THF.

Based on the assumption that the energy difference of 0.4 kcal mol^{-1} between the two 2,1-insertion ruthenacycle complexes (**D1$_{2,1}$** and **D2$_{2,1}$**) is small enough that both species are populated during the catalytic cycle, it is comforting to note that both ruthenacycle isomers preferentially form the *trans* 1,2-disubstituted alkene product over the *cis* stereoisomer. This agrees with experiment that only *trans* **3b** is observed, and is due to H transfer of different β-hydrogens (H$_a$ or H$_b$). The free-energy difference between **TS(D1-E1)1$_a$** and **TS(D2-E2)1$_a$** suggests a preference of about 10^4 for formation of the *trans* product over the *cis* isomer.

The absence of a di-alkenylated product (**3b$_{di}$**) formed during the reaction was investigated, with the subsequent C-H activation of **3b** at the remaining *ortho* C-H position modelled. The barrier for this activation was 15.4 kcal mol^{-1} (see Supporting Information, Table S2), 3 kcal mol^{-1} higher than activation of the initial C-H site in substrate **1b** (**TS(A-B)1** = +12.4 kcal mol^{-1}), hence **3b** does not undergo a second C-H activation. The unusual isomeric preference **1ar** / **1aq** substrates were likewise studied. Here, the major and minor C-H activation pathways were modelled for **1ar** (see Supporting Information, Table S3) and unsurprisingly the barrier for the major isomer pathway was lower in free energy, by 0.9 kcal mol^{-1}. This small difference, and similar energies for ^{1ar}**A** and ^{1ar}**A′**, the major and minor isomers of [Ru(*p*-cymene)(OAc)(**1ar**)]$^+$ respectively, (ΔG = 0.4 kcal mol^{-1}) agree with the experimental observation of both isomers, showing a slight energetic preference for the formation of the major isomer.

In order to estimate the Gibbs energy change for the uncatalyzed coupling of **1a** to **2b** to give **3b**, the oxidation process also needs to be included (equation 1). The overall reaction may be considered as:

$$\mathbf{1a} + \mathbf{2b} + \tfrac{1}{2}O_2 \rightarrow \mathbf{3b} + H_2O \qquad (1)$$

for which the exergonic Gibbs energy change (at 25 °C) is -49 kcal mol^{-1}. This is the amount by which all the Gibbs energies relative to **A** must be reduced between one turnover of the catalytic cycle and the next. (Note that the reaction path for the conversion from **E2$_{trans}$** to **A** in the next cycle has not been investigated computationally.) The significance of this consideration is that it allows the turnover-dependent intermediate and the turnover-dependent transition state to be identified as **D2$_{2,1}$** and **TS(D2-E2)1$_a$**, respectively, which occur sequentially within the same turnover cycle (Figure 7); the possibility of the turnover-dependent transition state occurring in the subsequent cycle can be discounted in this case.[20] Thus the computational modelling predicts the rate-determining step (as commonly understood) to be formation of the agostic intermediate immediately prior to β-hydride transfer. Under the experimental conditions the oxidation step is undoubtedly mediated by Cu(OAc)$_2$, although the detailed mechanism is unknown.[21] However, for the present purpose it is necessary only to consider overall stoichiometry and thermochemistry, not kinetics and mechanism for this stage of the turnover cycle. The calculated free energy changes ΔG_{MeTHF} reported above (Figures 2 – 6) refer to a standard state of 1 atm for all species, but detailed considerations of the rate-determining step (or, in general, of the turnover-dependent intermediate and transition state within a steady-state catalytic cycle)[20] depend upon actual concentrations under experimental conditions. The relative Gibbs energies shown in Figure 7 are corrected for the change from 1 atm (concentration c_1) to the standard reaction conditions (Table 1; concentration c_2) by the term $RT\ln(c_1/c_2)$ at temperature T = 120 °C. The ligand exchange step **B** → **C** (for which a transition structure has not been determined) becomes exergonic due to the larger relative concentration of alkene **2b**, with the consequence that the free energies of the transition structures for the alkene insertion and β-hydride transfer sections of the cycle are lowered with respect to those in the C-H activation section. The resulting profile (Figure 7) shows four transition structures (**TS(A-B)1**, **TS(A-B)2**, **TS(C2-D2)$_{2,1}$** and **TS(D2-E2)1$_a$**) all with quite similar free energies.

Kinetic Isotope Effects

Relative to **A**, the computational modelling predicts an intrinsic KIE k_{H5}/k_{D5} = 2.2 for the C-H activation step. Since the preceding transition structure **TS(A-B)1** for formation of the agostic intermediate is calculated to be slightly higher in energy, the intrinsic KIE would be partially masked, leading to a reduced value for the observed isotope effect. The experimental KIE by direct comparison of initial reaction rates for **1a** and **[D]$_5$-1a** has a value of about 2, which seems to suggest that most of the intrinsic KIE is being expressed. The KIEs calculated for the individual agostic formation, migratory insertion, and β-hydride elimination steps are all essentially unity as expected (Scheme 14).

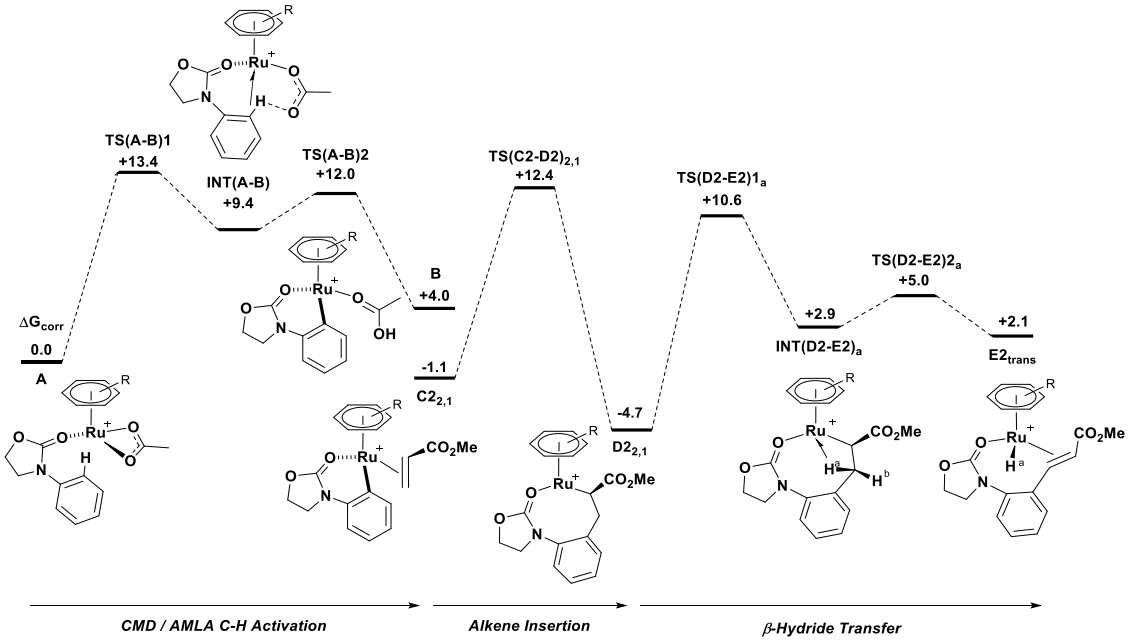

Figure 7: DFT calculated free energies (kcal mol^{-1} relative to **A**) for the coupling of **1a** and **2b** to form **3b** using a ruthenium catalyst at 120 °C in Me-THF and at concentrations corresponding to the standard experimental conditions (Table 1).

Scheme 14: Full Mechanism of Ruthenium-Catalyzed C-H Alkenylation including Kinetic and Energetic (kcal mol^{-1}) DFT Contributions

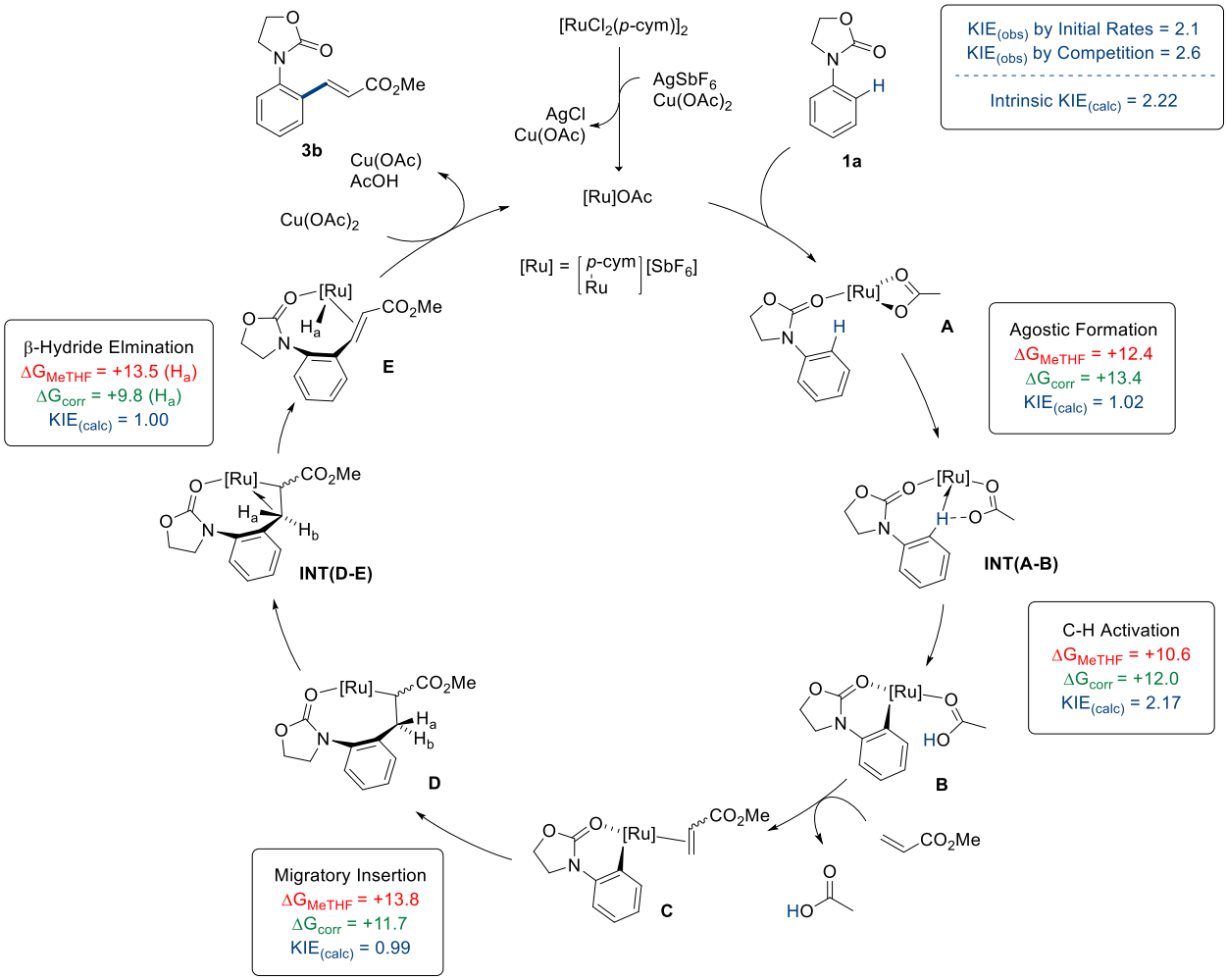

The KIE determined by the method of intermolecular competition expresses the isotopic discrimination up to the first irreversible step of the cycle, relative to free starting material. It is known that cyclometallation is reversible (Scheme 12), leading to loss of deuterium from the *ortho* position of **1a**. The product ratio determined in the competition experiment therefore reflects the isotope effect on cyclometallation. However, the interpretation of the experimental isotope effect is complicated by at least two factors. First, the isotopic product ratio observed depends upon the degree of conversion, since starting from a 1:1 mixture of isotopologues, a product ratio of 1:1 must be obtained for 100% conversion: the observed isotope effect should be corrected for the fractional degree of conversion, which leads to a greater value for the KIE.[22] Second, the fact that isotopic exchange at the *ortho* position is seen to take place during cyclometallation means that the proportion of deuterated **1a** in the reaction mixture is reduced, leading to an increase in the apparent value of the KIE. Numerical simulation shows that only a small percentage of isotopic exchange due to $\mathbf{B} \rightarrow \mathbf{A}$ reversibility is required to account for an apparent KIE of about 2.6 as observed for the intermolecular competition experiment.

CONCLUSION

We have reported the first use of the oxazolidinone directing group in ruthenium catalyzed C-H functionalization. This proof of concept of cyclometalation and subsequent functionalization was modeled on an alkenylation reaction. This led to the synthesis of over 25 novel substituted *N*-aryloxazolidinone motifs with up to 94% yields with absolute mono-selectivity. This methodology granted access to biologically relevant derivatives of oxazolidinone pharmaceuticals and could be applied to late stage drug modification.

DFT calculations for most sections of the catalytic cycle suggest why ***trans*-3b** is the only product isomer obtained, but yield very similar free energies for the transition states of several steps in the proposed mechanism using relative concentrations corresponding to the experimental conditions. The C-H activation step involves a KIE of $k_H/k_{D5} \approx 2$ in apparent agreement with the observed value, but several reasons are noted why a direct comparison between calculation and experiment may not be warranted.

ASSOCIATED CONTENT

Supporting Information. Full characterization, NMR spectra, computational data and crystallographic information is attached. This material is available free of charge via the Internet at http://pubs.acs.org.

AUTHOR INFORMATION

Corresponding Author

* Christopher G. Frost: C.G.Frost@bath.ac.uk (Synthetic)
* Ian H. Williams: I.H.Williams@bath.ac.uk (Physical Organic Computational)
* Claire L. McMullin: C.McMullin@bath.ac.uk (Inorganic Computational)

Notes

The authors declare no competing financial interest.

ACKNOWLEDGMENT

The authors gratefully acknowledge the University of Bath, Syngenta (JL) and the EPSRC (PW) for financial support. JL would also like to thank Christina Gulacsy and Dr. David Carbery for use and help with HPLC work, and John Lowe for NMR expertise. We thank the University of Bath for access to its High Performance Computing Facility.

REFERENCES

(1) For reading on linezolid see: (a) Barbachyn, M. R.; Ford, C. W. *Angew. Chem.* Int. Ed., **2003**, *42*, 2010-2023. (b) Gregory, W, A.; D. Brittelli, R.; Wang, C. L. J.; Wuonola, M. A.; McRipley, R. J.; Eustice, D. C.; Eberly, V. S.; Bartholomew, P. T.; Slee, A. M.; Forbes, M. *J. Med. Chem*. **1989**, *32*, 1673-1681. (c) Brickner, S. J.; Hutchinson, D. K.; Barbachyn, M. R.; Manninen, P. R.; Ulanowicz, D. A.; Garmon S. A.; Grega, K. C.; Hendges, S. K.; Toops, D. S.; Ford, C. W.; Zurenko, G. E. *J. Med. Chem*. **1996**, *39*, 673-679. (d) Evans, D. A.; Seidel, D.; Rueping, M.; Lam, H. W.; Shaw, J. T.; Downey, C. W. *J. Am. Chem. Soc*. **2003**, *125*, 12692-12693.
(2) For reading on tedizolid see: (a) Locke, J. B.; Finn, J.; Hilgers, M.; Morales, G.; Rahawi, S.; Kedar, G. C.; Picazo, J. J.; Im, W. B.; Shaw, K. J., Stein, J. L. *Antimicrob*. *Agents Chemother*. **2010**, *54*, 5337-5343. (b) Im, W. B.; Choi, S. H., Park, J. Y.; Finn, J.; Yoon, S. H. Eur. *J. Med. Chem*. **2011**, *46*, 1027-1039
(3) For reading on rivaroxaban see: (a) Roehrig, S.; Straub, A.; Pohlmann, J.; Lampe, T.; Pernerstorfer, J.; Schlemmer, K. H.; Reinemer, P.; Perzborn, E. *J. Med. Chem*. **2005**, *48*, 5900-5908. (b) Perzborn, E.; Roehrig, S.; Straub, A.; Kubitza, D.; Misselwitz, F. *Nature Reviews Drug Discovery*. **2011**, *10*, 61-75. (c) Yuan, J.; Liu, K.; Li, L.; Yuan, Y.; Liu, X.; Li, Y. *Molecules*, **2014**, *19*, 14999-15004, d) Rafecas, J. L.; Comely, A. C.; Ferrali, A.; Amelia Cortes, C.; Pasto Aguila, M. WO2011080341A1, **2011**.
(4) Moureau, F.; Wouters, J.; Vercauteren, D. P.; Collin, S.; Evrard, G.; Durant, F.; Ducrey, F.; Koenig, J. J.; Jarreau, F. X. *Eur. J. Med. Chem.* **1992**, *27*, 939-948.
(5) For reading on the synthesis and modification of *N*-aryloxazolidinones see: (a) Ghosh, A.; Sieser, J. E.; Riou, M.; Cai, W.; Rivera-Ruiz, L. *Org. Lett.*, **2003**, *5*, 2207–2210. (b) Mahy, W.; Plucinski, P.; Frost, C. G. *Org. Lett*., **2014**, *16*, 5020-5023. (c) Mallesham, B.; Rajesh, B. M.; Rajamohan Reddy, P.; Srinivas, D.; Trehan, S. *Org. Lett.*, **2003**, *5*, 963-965. (d) Mahy, W.; Plucinski, P.; Jover, J.; Frost, C. G. *Angew. Chem. Int. Ed*. **2015**, *127*, 11094-11098. (e) Mahy, W.; Leitch, J. A.; Frost, C. G. *Eur. J. Org. Chem.* **2016**, *7*, 1305-1313.
(6) For reviews on transition metal catalyzed C-H functionalization see: (a) Ackermann, L. *Chem. Rev.* **2011**, *13*, 3075-3078, (b) Arockiam, P. B.; Bruneau, C.; Dixneuf, P. *Chem. Rev*. **2012**, *112*, 5879−5918. (c) Chen, X.; Engle, K. M.; Wang, D-H.; Yu, J-Q. *Angew. Chem. Int. Ed*. **2009**, *48*, 5094–5115. (d) Engle, K. M., Mei, T-S.; Wasa, M.; Yu, J-Q. *Acc. Chem. Res.* **2012**, *45*, 788-802. (e) Rao, Y. Shan, G. Yang, X-L. *Sci. China Chem.* **2014**, *57*, 930-944. (f) Thirunavukkarasu, V. S.; Kozhushkov, S. I.; Ackermann, L. *Chem. Commun*, **2014**, *50*, 29-39.
(7) (a) Yamaguchi, J.; Yamaguchi, A. D.; Itami, K. *Angew. Chem. Int. Ed*. **2012**, *51*, 8960-9009 (b) Mahy, W.; Plucinski, P.; Jover, J.; Frost, C. G. *Angew. Chem. Int. Ed*. **2015**, *54*, 10944-10948. (c) Liu, P. M.; Frost, C. G. *Org. Lett*. **2013**, *15*, 5862-5865. (d) Brown, J. A.; Cochrane, A. R.; Irvine, S.; Kerr, W. J.; Mondal, B.; Parkinson, J. A.; Paterson, L. C.; Reid, M.; Tuttle, T.; Andersson, S.; Nilsson, G. N. *Adv. Synth. Catal*. **2014**, *356*, 3551-3562.
(8) For key seminal publications on directed ruthenium catalyzed C-H functionalization see: (a) Murai, S.; Kakiuchi, F. Sekine, S.; Tanaka, Y.; Kamatani, A.; Sonoda, M.; Chatani, N. *Nature*, **1993**, 366, 529-531 (b) Oi, S.; Fukita, S.; Hirata, N.; Watanuki, N.; Miyano, S.; Inoue, Y. *Org. Lett.* **2001**, *3*, 2579-2581. (c) Oi, S.; Ogino, Y.; Fukita, S.; Inoue, Y. *Org. Lett.* **2002**, *4*, 1783-1785. (d) Ackermann, L. *Org. Lett.* **2005**, *7* , 3123-3125. (e) Ackermann, L.; Althammer, A.; Born, R. *Angew. Chem. Int. Ed*. **2006**, *45*, 2619-2622, (f) Ackermann, L.; Vicente, R.; Althammer, A. *Org. Lett*. **2008**, *10*, 2299-2302. (g) Ozdemir, I.; Demir, S.; Cetinkaya, B.; Gourlaouen, C.; Maseras, F.; Bruneau, C.; Dixneuf, P. H., *J. Am. Chem. Soc.* **2008**, *130*, 1156-1157.
(9) For key examples of ruthenium catalyzed C-H functionalization using weakly coordinating directing groups see: (a) De Sarkar S.; Liu, W.; Kozhushkov, S. I.; Ackermann, L. *Adv. Synth. Catal*. **2014**, *356*, 1461-1479. (b) Ueyama, T.; Mochida, S.; Fukutani, T.; Hirano, K.;

Satoh, T.; Miura, M. *Org. Lett.* **2011**, *13*, 706-708. (c) Ackermann, L.; Pospech, J. *Org. Lett.* **2011**, *13*, 4153-4155. (d) Kakiuchi, F.; Kan, S.; Igi, K.; Chatani, N.; Murai, S. *J. Am. Chem. Soc.* **2003**, *125*, 1698-1699. (e) Bhanuchandra, M.; Yadav, M. R.; Rit, R. K.; Kuram, M. R.; Sahoo, A. K. *Chem. Commun.* **2013**, *49*, 5225-5227. (f) Padala, K.; Jeganmohan, M. *Org. Lett.* **2012**, *14*, 1134-1137. (g) Ackermann, L.; Lygin, A. V.; Hofmann, N. *Angew. Chem. Int. Ed.* **2011**, *50*, 6379-6382. (h) Graczyk, K.; Ma, W.; Ackermann, L. *Org. Lett.* **2012**, *14*, 4110-4113. (i) Padala, K.; Jeganmohan, M. *Org. Lett.* **2011**, *13*, 6144-6147. (j) Reddy, M. C.; Jeganmohan, M. *Chem. Commun.* **2014**, *51*, 10738-10741. (k) Li, J.; Kornhaass, C.; Ackermann, L. *Chem. Commun.*, **2012**, *48*, 11343-11345.

(10) (a) Kalyani, D.; Deprez, N. R.; Desai, L. V.; Sanford, M. S. *J. Am. Chem Soc.* **2005**, *127*, 7330-7331. (b) Yeung, C. S.; Dong, V. M. *Synlett*, **2011**, *7*, 974-978

(11) For palladium see: Leow, D.; Li, G.; Mei, T-S.; Yu, J-Q, *Nature*, **2012**, *486*, 518-522. For rhodium see: Colby, D. A.; Bergman, R. G.; Ellman, J. A. *Chem Rev*, **2010**, *110*, 624-655.

(12) (a) Pace, V.; Hoyos, Fernandez, M.; P.;Sinisterra, J. V.; Alcantara, A. R. *Green Chem.* **2010**, *12*, 1380-1382. (b) Pace, V.; Hoyos, P.; Castoldi, L.; De Maria, P. D.; Alcantara, A. R. *Chemsuschem*, **2012**, *5*, 1369-1379

(13) (a) **Crystal Data** for $C_{14}H_{14}FNO_4$ (compound **3aq$_1$**): M =279.26 g mol^{-1}, triclinic, space group P-1 (no. 2), a = 6.8220(2), b = 10.6058(3), c = 19.5239(7) Å, α = 105.484(3), β = 90.601(3), γ = 102.910(2)°, U = 1323.22(7) Å^3, Z = 4, T = 150.00(10) K, μ(Cu-Kα) = 0.954 mm^{-1}, D_c = 1.402 g cm^{-3}, 13114 reflections measured (8.9° ≤ 2θ ≤ 143.942°), 5164 unique (R_{int} = 0.0248, R_{sigma} = 0.0279) which were used in all calculations. The final R1 was 0.0379 (I > 2σ(I)) and wR_2 was 0.0994 (all data). (b) **Crystal Data** for $C_{14}H_{14}FNO_4$ (compound **3aq$_2$**): M =279.26 g mol^{-1}, tetragonal, space group $P4_32_12$, a = 9.43321(9), c = 29.5288(4) Å, U = 2627.64(6) Å^3, Z = 8, T = 150.00(10) K, μ(Cu-Kα) = 0.960 mm^{-1}, D_c = 1.412 g cm^{-3}, 23288 reflections measured (9.844° ≤ 2θ ≤ 143.71°), 2586 unique (R_{int} = 0.0317, R_{sigma} = 0.0148) which were used in all calculations. The final R1 was 0.0283 (I > 2σ(I)) and wR_2 was 0.0720 (all data). CCDC 1479666-1479667 (for 3aq$_1$ and 3aq$_2$, respectively) contain the supplementary crystallographic data for this paper. These data can be obtained free of charge via http://www.ccdc.cam.ac.uk/conts/retrieving.html, or from the Cambridge Crystallographic Data Centre, CCDC, 12 Union Road, Cambridge CB2 1EZ, UK.

(14) Liu, W.; Ackermann, L. *Chem. Commun.* **2014**, *50*, 1878-1881

(15) (a) Sova, M. *Mini. Rev. Mec. Chem.*, **2012**, *12*, 749-767 (b) Seelolla, G.; Cheera, P.; Ponneri, V. *Med. Chem.*, **2014**, *4*, 778-783

(16) For previous use of the pyrolidinone directing group in palladium catalyzed C-H functionalization see: (a) Giri, R.; Lam, J. K.; Yu, J-Q. *J. Am. Chem. Soc*, **2010**, *132*, 686-693. (b) Bedford, R. B.; Mitchell, C. J.; Webster, R. L. *Chem. Commun.* **2010**, *46*, 3095-3097. (c) Desai, L. V.; Malik, H. A.; Sanford, M. S. *Org. Lett.* **2006**, *8*, 1141-1144. (d) Prakash, G. K. S.; Mathew, T.; Hoole, D.; Esteves, P. M.; Wang, Q.; Rasul, G.; Olah, G. A. *J. Am. Chem. Soc*. **2004**, *126*, 15770-15776.

(17) Simmons, E. M.; Hartwig, J. F. *Angew. Chem. Int. Ed.*, **2012**, *51*, 3066-3072.

(18) DFT calculations were run with Gaussian 09 (Revision D.01). Ru centers were described with the Stuttgart RECPs and associated basis sets, and 6-31G** basis sets were used for all other atoms. Full details and references for all computational methods can be found in SI.

(19) Algarra, A. G.; Davies, D. L.; Khamker, Q.; Macgregor, S.; McMullin, C. L.; Singh, K.; Villa-Marcos, B. *Chem. Eur. J.*, **2015**, *21*, 3087-3096.

(20) (a) Kozuch, S.; Shaik, S. *Acc. Chem. Res*. **2010**, *44*, 101-110. (b) Kozuch, S.; Martin, J. M. L. *ACS Catal.* **2012**, *2*, 2787-2794.

(21) Funes-Ardoiz, A.; Maseras, F. *Angew. Chem. Int. Ed.*, **2016**, *55*, 2764-2767

(22) Melander, L.; Saunders, W. H. *Reaction Rates of Isotopic Molecules*, Wiley, New York, 1980, 56-129